

# A ROSAT pointed observation of the Chamaeleon II dark cloud\*

J.M. Alcalá<sup>1,6</sup>, E. Covino<sup>1</sup>, M.F. Sterzik<sup>2</sup>, J.H.M.M. Schmitt<sup>3</sup>, J. Krautter<sup>4</sup>, and R. Neuhäuser<sup>5</sup>

<sup>1</sup> Osservatorio Astronomico di Capodimonte, 80131 Napoli, Italy

<sup>2</sup> European Southern Observatory, Casilla 19001, Santiago 19, Chile

<sup>3</sup> Hamburger Sternwarte, Gojenbergsweg 112, 21029 Hamburg, Germany

<sup>4</sup> Landessternwarte Königstuhl, 69117 Heidelberg, Germany

<sup>5</sup> Max-Planck-Institut für Extraterrestrische Physik, 85740 Garching, Germany

<sup>6</sup> Instituto Nacional de Astrofísica, Óptica y Electrónica, A.P. 51 y 216 C.P. 72000, Puebla, México

Received 23 September 1999 / Accepted 13 January 2000

**Abstract.** A deep 13.5 ksec ROSAT PSPC pointed observation in the Chamaeleon II (Cha II) cloud is reported. 40 X-ray sources are detected of which 14 can be identified with previously known young stellar objects (YSOs), namely IRAS sources, classical T Tauri stars and weak T Tauri stars. From spectroscopic follow-up observations, four new weak T Tauri candidates have been found. The X-ray sources are mainly located on the north-east of the cloud and their spatial distribution follows the lanes of the 100 $\mu$ m dust emission. Their X-ray properties are similar to those of low-mass PMS stars. None of the protostar candidates in Cha II has been detected in the ROSAT pointed observation, in agreement with the ASCA observations results. The X-ray detection rates indicate that the weak T Tauri stars (WTTS) are less numerous than the classical T Tauri stars (CTTS), contrarily to the findings in Chamaeleon I (Cha I) and other star forming regions where the WTTS may outnumber the CTTS. The latter result could be a consequence of the fact that Cha II is in an earlier evolutionary stage as compared to Cha I, as conjectured by previous studies. The Cha II young stellar objects (YSOs) are, on the average, slightly less X-ray luminous than those in Cha I, but the normalised X-ray luminosity distribution functions of the two regions are not significantly different.

**Key words:** surveys – stars: formation – stars: low-mass – stars: pre-main sequence – ISM: individual objects: Chamaeleon clouds – X-rays: stars

## 1. Introduction

X-ray surveys in star forming regions (SFR) have been very successful on finding X-ray emitting pre-main sequence stars (Montmerle et al. 1983; Walter et al. 1988; Feigelson and Kriss 1989; Krautter et al. 1994; Walter et al. 1999). However, the X-ray detection rate of strong infrared (IR) sources (or class-I IR sources), normally associated with embedded young stellar ob-

jects (YSOs), is much lower than the detection rate of classical T Tauri stars (CTTS or class-II IR sources) and weak T Tauri stars (WTTS or class-III IR sources). Casanova et al. (1995) report a deep (33.4 ksec) ROSAT pointed observation in the central part of the  $\rho$  Ophiuchi SFR. Most of their X-ray sources could be identified with class-II and class-III IR sources, but between two and four sources might be class-I proto-stars. They predict that many (up to 200) low-mass X-ray emitting YSOs may exist in the  $\rho$  Ophiuchi SFR. They claim that the X-ray emission of these stars may have a very important impact which probably provides a negative feedback on star formation in the denser parts of the  $\rho$  Ophiuchi cloud. This effect may play an important role in the self-regulation of low-mass star formation in molecular clouds. Other authors also claim the X-ray detection of class-I protostars in the Cr A dark clouds and NGC 1333 (Koyama et al. 1994, 1996; Grosso et al. 1997; Kamata et al. 1997; Neuhäuser & Preibisch 1997).

The southern star forming region (SFR) in Chamaeleon consists of three main dark clouds named Cha I, Cha II and Cha III (Hoffmeister 1963). Another relatively small cloud, located between Cha I and Cha II is also part of the complex. Because of its proximity, the Chamaeleon SFR is an ideal place to study low-mass star formation. The X-ray properties of the Cha I members have been investigated by Feigelson et al. (1993) and by Alcalá et al. (1997).

At a distance of about 200 pc (Hughes and Hartigan 1992), the Cha II dark cloud is well characterised by the presence of H $\alpha$  emission line objects (Schwartz 1991; Hartigan 1993) as well as of embedded class-I and class-II sources (Whittet et al. 1991; Prusti et al. 1992; Larson et al. 1998). Therefore, Cha II is an ideal laboratory to study the X-ray emission from protostars and low-mass young stellar objects, and the interaction of the X-ray photons with the interstellar gas. The PMS population in Cha II has been characterised by Gauvin and Strom (1992) and Hughes and Hartigan (1992).

The first X-ray observations in the Cha II dark cloud were carried out during the ROSAT all-sky survey (RASS). Ten X-ray sources were detected in the general direction of Cha II during the RASS, with two of them being identified with new class-

---

Send offprint requests to: J.M. Alcalá

\* Based on observations with the European Southern Observatory, La Silla, Chile under proposal number 55.E-0792

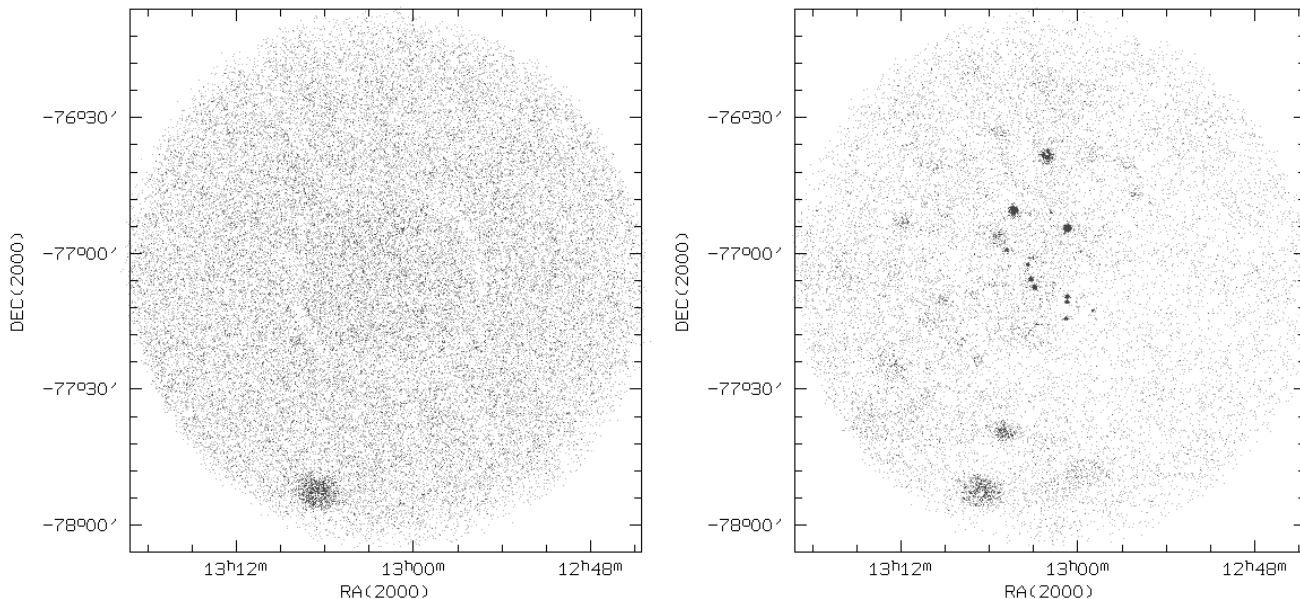


**Fig. 1.** Soft (0.1-0.5 keV, left panel) and hard (0.5-2.5 keV, right panel) ROSAT images in the direction of the Cha II dark cloud.

III, PMS stars (Alcalá et al. 1995; Covino et al. 1997). In an X-ray observation of Cha II carried out by the ASCA satellite, eight X-ray sources were detected with high confidence level but, none of the class I IR sources or protostar candidates was detected (Yamauchi et al. 1998).

In order to further study and characterise the X-ray emitting population of the Cha II dark cloud, we have carried out a 13.5 ksec PSPC ROSAT pointed observation. In this paper, we report the X-ray sources detected, their optical identification with YSOs in Cha II as well the X-ray properties of the PMS population. The analysis of X-ray spectra and light curves are deferred to a forthcoming paper.

In Sect. 2, the X-ray pointed observation as well as the detection of the X-ray sources are discussed. The identification of the X-ray sources is reported in Sect. 3 and the results regarding detection rates, spatial distribution and X-ray properties are reported in Sect. 4. Finally, in Sect. 5 the discussion and conclusions are presented.

## 2. The ROSAT observation and source detection

The 13.5 ksec ROSAT PSPC pointing observation in Cha II was centered in  $RA(2000) = 13^h02^m0^s$  and  $DEC(2000) = -77^\circ04'12''$  and was carried out from September 10 to 17, 1993. The Cha II dark cloud has the right size, of about 1.5 square degrees, to be practically entirely covered in a single PSPC pointing.

The reduction and subsequent analysis of the X-ray data were performed following the pipelines of the Extended Scientific Analysis System (EXSAS). The sources are identified by an excess of photons in comparison with both a local and a global background using a “maximum likelihood” method. For a detailed description of the steps of the reduction we refer to Alcalá et al. (1995). We have fixed the detection threshold to the

value of  $L=7^1$ . This might produce some spurious sources, but we can reach lower X-ray fluxes. In this way, 40 X-ray sources were detected in our ROSAT pointing in Cha II. The RXJ designation, coordinates, count rate, as well as exposure time and maximum likelihood of each X-ray source are listed in Table 1. Following the notation by Feigelson et al. (1993) for the Cha I cloud, we call these sources “CHIIXR”. We find that the typical error box for bright sources has a radius of about  $3''$ , while for the faintest may be as high as  $30''$ .

In Fig. 1 the soft (0.1-0.5 keV) and the hard (0.5-2.5 keV) ROSAT images are shown (left and right panel respectively). Except for one source, located almost at the lower border of the PSPC window and identified with the bright star HD113513 (unrelated to Cha II, see Sect. 3), almost all the X-ray sources are detected only in the hard energy band. This means that most of the soft X-ray photons are absorbed or that the sources are intrinsically hard.

## 3. Source identification

Fourteen of the 40 X-ray sources detected can be identified with previously known objects. The counterparts of the X-ray sources are listed in Tables 1 and 4. These are mainly IRAS sources, CTTS and WTTS found in previous  $H\alpha$  surveys (Schwartz 1977; Whittet et al. 1991; Prusti et al. 1992; Hartigan 1993;

<sup>1</sup> The likelihood is defined as  $L = -\ln(P)$ , where  $P$  is the probability that the observed distribution of photons comes from a spurious background fluctuation. This distribution is estimated using Poisson statistics. The choice of the threshold for a significant source detection depends on how many spurious sources one wants to accept. A conservative value for the detection threshold is 10 which corresponds to  $P = 4.54 \times 10^{-5}$ . A value of  $L = 10$  leads to an expected number of spurious sources in the range of 0.7–2.3 (Zimmermann et al. 1993, p. 5–112).

**Table 1.** X-ray sources detected in the ROSAT pointed observation of the Chamaeleon II dark cloud.

RXJ	CHIIXR	RA(2000)	DEC(2000)	rate	Exp.	ML	ident/notes
			cts/ksec	[ksec]			
1256.6–7646	1	12 56 34.7	-76 46 08.6	3.5±0.7	13.0	28.1	Sz 46N1
1257.1–7639	2	12 57 10.1	-76 39 48.7	2.9±0.8	11.6	10.8	IRAS12535-7623, L13
1259.1–7712	3	12 59 10.9	-77 12 06.2	1.5±0.4	13.1	34.2	faint object (= IRAS 12551-7657 ?)
1259.5–7637	4	12 59 26.4	-76 37 39.1	3.2±0.9	11.2	10.1	A2, very faint object in the X-ray center.
1300.1–7659	5	13 00 03.1	-76 59 00.9	0.8±0.3	12.6	14.3	empty box
1300.2–7748	6	13 00 10.4	-77 48 06.7	7.3±1.6	14.2	15.9	faint object at about 20" NE
1300.9–7708	7	13 00 52.6	-77 08 58.5	1.2±0.3	13.2	40.7	Sz 48NE
1300.9–7710	8	13 00 55.6	-77 10 15.5	6.4±0.8	13.3	252.0	Sz 50 S12571-7654-m
1300.9–7654	9	13 00 56.5	-76 54 02.0	95.8±3.0	12.8	5335.3	RXJ 1301.0-7654a , A3
1301.0–7713	10	13 00 58.3	-77 13 57.1	4.1±0.6	13.4	152.2	F12571-7657
1301.9–7706	11*	13 01 50.2	-77 06 00.0	0.5±0.2	13.3	11.2	new WTTS candidate, SpT = K1
1302.0–7650	12	13 01 59.5	-76 50 19.1	1.7±0.4	12.7	25.4	IRAS12583-7634
1302.3–7637	13	13 02 15.1	-76 37 57.0	24.3±1.8	13.2	320.1	CM Cha = IRAS12584-7621, L22, A4
1302.6–7719	14	13 02 38.0	-77 19 19.4	0.8±0.3	13.3	8.9	12587-7706 ??, offset = 110"
1302.7–7711	15	13 02 41.8	-77 11 11.3	0.5±0.2	13.2	7.7	faint objects in field, Galaxies? spurious source ?
1302.8–7705	16	13 02 48.6	-77 05 39.8	0.5±0.2	13.1	8.0	faint objects in field center
1303.0–7715	17*	13 02 57.5	-77 15 14.2	1.3±0.4	13.2	19.1	UNS
1303.1–7706	18	13 03 03.7	-77 06 59.1	35.7±1.8	13.2	2033.2	RXJ1303.1-7706, A5
1303.2–7700	19*	13 03 10.4	-77 00 31.5	1.2±0.4	13.1	20.3	UNS
1303.3–7705	20	13 03 18.3	-77 05 16.8	16.0±1.2	13.2	747.6	cluster of galaxies GAL303.65-1425
1303.4–7650	21*	13 03 22.0	-76 50 45.7	0.7±0.3	12.6	8.8	UNS
1303.4–7716	22	13 03 23.7	-77 16 46.7	2.0±0.6	13.2	8.1	star some 20" SW of X-ray center
1303.5–7645	23	13 03 30.0	-76 45 02.6	1.2±0.5	10.0	9.7	faint objects close to center
1303.5–7701	24*	13 03 30.6	-77 01 58.6	4.9±0.7	13.2	167.9	new WTTS candidate, SpT = G7
1303.7–7717	25	13 03 42.0	-77 17 58.3	0.8±0.3	13.5	10.3	empty box
1304.3–7716	26	13 04 15.5	-77 16 04.9	2.1±0.6	13.4	11.7	faint objects in the center
1304.4–7650	27	13 04 23.7	-76 50 02.5	49.7±2.5	10.5	1294.2	Hn 23, Hn22, IRAS13005-7633, L2, A6
1304.9–7658	28*	13 04 54.0	-76 58 46.9	3.2±0.6	13.6	55.0	UNS
1305.1–7657	29	13 05 03.2	-76 57 03.0	0.7±0.3	13.3	9.3	BE Cha
1305.2–7738	30	13 05 13.2	-77 38 59.3	29.4±2.2	12.2	234.7	BF Cha = Sz54 = IRAS 13014-7723, A7
1305.3–7632	31	13 05 17.3	-76 32 43.7	4.3±1.1	13.1	13.0	star some 30" SW of center
1305.5–7655	32	13 05 29.4	-76 55 30.8	5.6±0.9	13.3	29.9	faint star some 10" S from center
1306.8–7752	33*	13 06 45.8	-77 52 00.9	154.4±6.1	13.8	694.6	HD113513 (UNS)
1307.0–7722	34	13 06 56.8	-77 22 57.3	2.3±0.6	13.2	17.0	Sz 57, A8
1307.3–7708	35*	13 07 15.4	-77 08 14.8	0.8±0.3	13.0	8.0	new WTTS candidate, SpT = G6
1308.0–7708	36*†	13 08 00.3	-77 18 46.4	5.3±1.2	11.9	16.4	HD113696 (UNS),
1309.5–7709	37	13 09 10.5	-77 09 27.1	3.7±0.8	12.6	19.8	F13052-7653, L30
1309.8–7639	38	13 09 22.9	-76 39 46.5	2.3±0.8	13.9	7.8	empty box, spurious source ?
1311.5–7651	39*	13 11 31.7	-76 51 59.1	6.5±1.2	13.4	28.6	new WTTS candidate, SpT = K0
1312.5–7723	40	13 12 29.6	-77 23 53.6	7.1±1.6	12.0	14.5	faint star some 30" N from center

Notes to table:

\* : source investigated spectroscopically; UNS : unrelated nearby star resulted from spectroscopic observations, but the corresponding error circle still contains objects fainter than the magnitude limit for our spectroscopic observations; A# : ASCA sources by Yamauchi et al. 1998; L# : IR sources by Larson et al. 1998; † : for this source there is another possible counterpart, not observed spectroscopically, closer to X-ray center.

Larson et al. 1998) and on the basis of the RASS (Alcalá et al. 1995).

Seven of the eight sources detected in the ASCA observations by Yamauchi et al. (1998) were confirmed detections in the ROSAT pointing. Their source Nr. 1, identified with the Herbig Ae candidate IRAS 12496-7650, was not detected in our deep ROSAT pointing. The source CHIIXR-4 can be identified with the ASCA source No. 2, for which Yamauchi et al. (1998) find no optical counterpart. By inspection of the Digitised Sky Sur-

vey (DSS) field, we find that there is a faint object very close to the coordinates of CHIIXR-4, which might be the optical counterpart. Since the ASCA error box is about 1', it is most likely that such object is the counterpart of the ASCA source No. 2 by Yamauchi et al. (1998) as well.

The sources CHIIXR-9, CHIIXR-27 and CHIIXR-34 have ambiguous identifications, in the sense that there is more than one possible counterpart. However, in the case of CHIIXR-9 we think that the optical counterpart is the RASS WTTS

RXJ 1301.0–7654a identified by Alcalá et al. (1995) instead of Sz 49, since its offset position is about  $3''$ , while Sz 49 is located farther away at about  $15''$  from the X-ray position. In the case of CHIIXR-27, there are two TTS candidates as possible counterparts: Hn22 and Hn23, discovered by Hartigan (1993) in a CCD objective-prism survey. These two stars are separated by  $6.5''$  and, interestingly, both candidates are classified as CTTS on the basis of their  $H\alpha$  emission line equivalent width ( $30\text{\AA}$  and  $24\text{\AA}$ , respectively; Hartigan 1993). These stars are very likely the counterparts for the infrared source IRAS 13005-7633. Sz 57 and Sz 58 may be associated to the source CHIIXR-34 although Sz 57 is closer to the X-ray position.

The sources CHIIXR-2, 13 and 37 can be identified with the class-II infrared sources IRAS12535-7623, IRAS12584-7621 (CM Cha) and IRAS-F13052-7653 by Larson et al. (1998). The X-ray sources CHIIXR-10 and CHIIXR-12 might be associated with the infrared sources IRAS F12571-7657 and IRAS 12583-7634 respectively. By inspection of the ESO/SRC plates, Prusti et al. (1992) found that the IRAS error box of the former IR source is empty, but they could confirm that its IR colours are those of a class-II IR source. On the other hand, IRAS 12583-7634 has been only detected in the  $100\mu\text{m}$  IRAS band (Schwartz 1991).

The X-ray source CHIIXR-3 might be associated with the infrared source IRAS 12551-7657 but, since the IR coordinates are rather uncertain, the identification should be taken with care. By inspection of the DSS field, we find that there is a faint star to the north-east of the IRAS source which practically coincides with the X-ray position.

The source CHIIXR-14 is located close to the infrared source IRAS 12589-7646 but the coordinate offset is large ( $\approx 100''$ ) and hence, it cannot be the counterpart of the IRAS source. The X-ray boxes of the sources CHIIXR-5 and CHIIXR-25 are empty and the sources CHIIXR-38 and CHIIXR-15 might be spurious, given their low ML values.

Finally, source CHIIXR-20 might be identified with the cluster of galaxies Gal 303.65-1425.

### 3.1. Spectroscopic observations

In order to complete the identification of the X-ray sources, the 10 sources, marked with a “\*” in Table 1 were investigated spectroscopically during two nights in April 1995, using the Boller & Chivens spectrograph attached to the ESO 1.5m telescope. The observational method and the reduction of these spectra are described in Alcalá et al. (1995). The nominal resolution of the spectra, as measured from several isolated lines of the HeAr comparison spectrum, is  $3.5\text{\AA}$  FWHM.

The main goal of these observations was the search for new X-ray emitting WTTS by means of the identification of the Li I  $6708\text{\AA}$  absorption line. The identification of PMS stars by means of the lithium line in intermediate resolution spectra has been matter of controversy (Briceño et al. 1997; Favata et al. 1997). However, the effectiveness in identifying PMS stars on this basis has been proven by recent high-resolution studies (Covino et al. 1997; Wichmann et al. 1999; Alcalá et al. 1999).

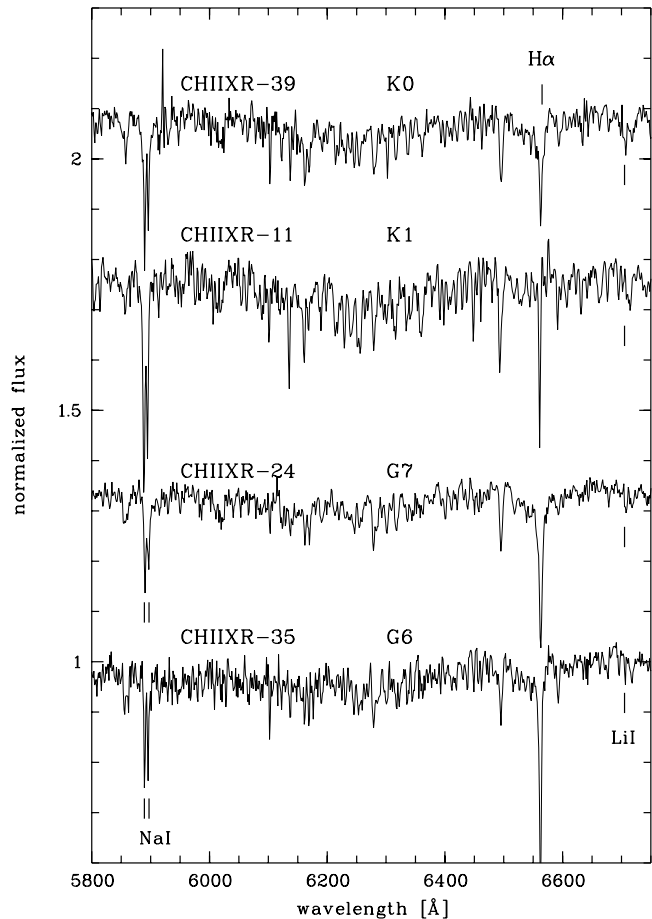


**Fig. 2.** Optical spectra of new X-ray emitting WTTS candidates in Cha II. The spectral type, determined as explained in Sect. 3.2, is indicated.

In any case, due to the blend of the Li I  $6708\text{\AA}$  line with the nearby Fe lines this spectra are used only for the detection of the lithium feature and not for the measurement of line equivalent width.

Three stars, associated to the sources CHIIXR-24, 35 and 39, show the Li I  $6708\text{\AA}$  absorption line in their optical spectra (c.f Fig. 2). The  $H\alpha$  line of these stars is seen in absorption, but in the case of CHIIXR-39, a partial filling in of the line is observed, indicating some chromospheric activity. For the star associated to the source CHIIXR-11 the lithium line is found to be in blend with the Ca I  $6718\text{\AA}$  line. Hence, this star might be either an ultra-fast rotator or an unresolved spectroscopic binary.

Spectral types have been assigned to these stars following the procedure described in previous papers (Covino et al. 1997; Alcalá et al 2000). The spectral types are also reported in Table 1. We consider these stars as new WTTS candidates but high-resolution spectroscopic observations are needed to confirm that their lithium line is stronger than in active ZAMS stars of the same spectral type and to investigate whether their radial velocities are consistent with the mean for the Cha II cloud.

The observed stars in the error box of the other sources (CHIIXR-17, 19, 21, 28 and 36) are apparently unrelated to Cha II. However, we stress that, because of the magnitude limit ( $V \approx 16.5$ ) of our spectroscopic observations, only the brightest stars in the X-ray error boxes could be observed. Therefore, we cannot exclude that other faint objects are the true optical counterparts of these sources. In the case of CHIIXR-33, the X-ray coordinates match well with those of the G5V star HD113513, but lithium was not detected in this star.

The remaining X-ray boxes contain objects fainter than our limit of  $V \approx 16.5$  mag and, hence, deserve further spectroscopic studies in order to investigate whether their spectra are those of PMS stars. The notes in Table 1 give information regarding the inspection of the DSS fields.

## 4. Results

Of the 49 PMS stars and IRAS sources in Cha II (see the compilation in Table 4), 47 fall in the area of our ROSAT pointing. The CTTS Sz64 and the IRAS source IRAS 13047-7750 (detected only in  $100\mu\text{m}$ : Schwartz 1991) lie outside the area of the pointing (c.f. Fig. 3). We report now the results of the X-ray detection rates, the spatial distribution of the X-ray sources and their X-ray luminosities.

### 4.1. Detection rates

There are 5 known class-I deeply embedded IRAS sources, possibly protostars, in Cha II, namely IRAS 12500-7658, IRAS 12496-7650, IRAS 12533-7632, IRAS 12553-7651 and IRAS 13036-7644 (Whittet et al. 1991; Prusti et al. 1992). The number of known class-II sources or CTTS in Cha II is about 30 (Whittet et al. 1991; Prusti et al. 1992; Hartigan 1993; Larson et al. 1998). Prior to ROSAT, only two class-III sources or WTTS were known (Hn24 and Hn26 by Hartigan 1993) in Cha II which, curiously, were not detected in our deep ROSAT pointing. Two new WTTS found on the basis of the RASS have confirmed detections in the ROSAT pointing

In a near-infrared study of 18 IRAS sources in Cha II, Larson et al. (1998) find that 14 can be classified as field class-III IR sources unrelated to Cha II; only 4 can be classified as class-II sources with infrared properties that match well those of CTTS. These four objects, namely IRAS 12535-7623, IRAS 12584-7621 (=CM Cha), IRAS 13005-7633 (= Hn22 & Hn23), and IRAS F13052-7653, are detected in X-rays (see Sect. 3). Thus, the fact that the 14 field class-III sources were not detected in X-rays gives support to the conclusion by Larson et al. (1998) that they are unrelated to the Cha II cloud.

The X-ray detection rates are summarised in Table 2. In the first column, the different IR classes of objects, namely class I IR sources, CTTS, WTTS and other IR sources (whose association with the Cha II cloud needs to be confirmed) are listed; in the second column the number of X-ray detected objects of each IR class is reported. The numbers of additional X-ray sources identified in this work, for which association to the Cha II cloud

**Table 2.** Summary of X-ray detections

IR-Class	No. of X-ray detections	Fraction <sup>†</sup>
I	0	0
II	11	22%
III	2 (11)	4% (22%)
other IR sources	1 (1)	2% (2%)

<sup>†</sup> the percentage was determined by normalization of each number to the 49 YSOs of Cha II (listed in Table 4).

needs confirmation, are given in parenthesis; the fraction of X-ray detected objects, eg. the number of X-ray detected objects of each IR class normalized to the total of 49 known YSOs in Cha II (see also Table 4), is listed in the third column. The detection rates are as follows (see also Table 4): None of the deeply embedded class I IR sources was detected in the ROSAT deep pointing, in agreement with the result from ASCA observations by Yamauchi et al. (1998); 11 class-II sources or CTTS, were detected; finally the 2 RASS discovered class-III objects or WTTS were detected.

The numbers above would indicate that the CTTS are the most abundant among the X-ray emitting low-mass PMS stars in the Cha II cloud. If the four new lithium stars, found in the spectroscopic identifications (see Sect. 3.1) are confirmed to be PMS stars, the number of WTTS detected would rise to 6 which is still smaller than the number of X-ray detected CTTS. Additional low-mass PMS stars are expected to be found as counterparts of the sources not yet investigated spectroscopically: from inspection of the DSS fields (see Table 1) and from the X-ray hardness ratios (see Sect. 5), we expect some 7 additional potential candidates. Therefore, the number of WTTS detected in our ROSAT pointing would rise to about 13, which would be comparable to the number of X-ray detected CTTS.

In other SFRs, it has been found that the WTTS may outnumber the CTTS by a factor running from 2 to 10 (Walter et al. 1988; Feigelson et al. 1993; Krautter et al. 1994), depending on the completeness of the surveys, in X-ray flux and spatial extent. In the Cha I cloud, the WTTS are a factor of about 2 more numerous than the CTTS (Lawson, Feigelson and Huenemoerder 1996). In Cha II the total number of class-II sources is about 30. Therefore, a remarkable result of our deep ROSAT observation in Cha II is that the number of WTTS may be at most about half of the total number of CTTS.

### 4.2. Spatial distribution

The spatial distribution of the ROSAT X-ray sources detected in Cha II is shown in Fig. 3. The spatial distribution of the previously known T Tauri stars and IRAS sources in Cha II is also shown for comparison. The  $17 \text{ MJy sr}^{-1}$  contour, which more or less defines the limits of the cloud, is represented by a thick shaded line.

Most of the optically visible PMS stars and infrared sources in Cha II are located on the north-east and south edges of the cloud (c.f. Fig. 3). The ROSAT X-ray sources tend to occupy

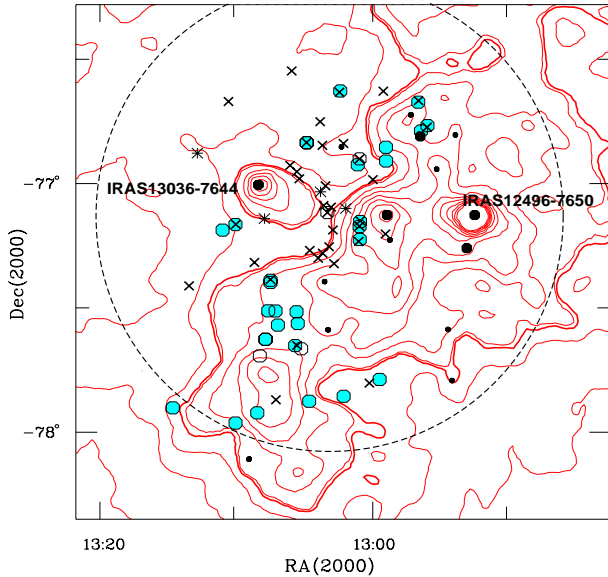


**Fig. 3.** Spatial distribution of the X-ray sources detected in the ROSAT pointed observation and of TTS and IRAS sources in the Chamaeleon II cloud. The X-ray sources are represented with “x” symbols. The four newly identified lithium stars (see Sect. 3.1) are marked with an asterisk. The previously known class-III and class-II IR sources are represented with open and shaded circles respectively. The class-I IR sources are indicated as large black dots, while other IRAS sources, detected normally only in  $100\mu\text{m}$  and lacking other IR colours, are represented with small dots. The contours, from 10 to  $40 \text{ MJy sr}^{-1}$  in steps of  $2.5 \text{ MJy sr}^{-1}$ , of the  $100\mu\text{m}$  dust emission revealed by the IRAS satellite are also drawn. The thick contour corresponds to  $17 \text{ MJy sr}^{-1}$ . The big dashed circle indicates the ROSAT window.

those regions too. Interestingly, there is a concentration of X-ray sources at about  $RA = 13^{\text{h}}03^{\text{m}}$  &  $DEC = -77^{\circ}08'$  that follows the lanes of the dust emission. These sources are located where the gas density gradient is highest, between the main Cha II cloud and the clump where IRAS 13036-7644 is located. The fact that the sources are detected in such a gap might be due to an extinction effect. Note that three of the four newly identified lithium stars, marked with an asterisk in Fig. 3, are located in that area. Therefore, many of the counterparts of the X-ray sources located in the same area are expected to be PMS stars too.

The region limited by  $12^{\text{h}} : 40^{\text{m}} < RA < 12^{\text{h}} : 55^{\text{m}}$  and  $-78^{\circ}40' < DEC < -76^{\circ}30'$ , in which the candidate protostar IRAS 12496-7650 lies, is devoid both in X-ray sources and optically visible PMS stars. A high extinction with  $A_V \geq 20 \text{ mag}$  in that part of the cloud may be expected and hence, the fact that only a few embedded IRAS sources, not detected in X-rays, are found in that part of the cloud, might also result from an extinction effect.

#### 4.3. The X-ray luminosities

For a given source, the X-ray luminosity, assuming isotropic radiation, can be computed as  $L_X = 4 \cdot \pi \cdot d^2 \cdot f_X$ , where  $d$  is the distance and  $f_X$  is the X-ray flux at the earth in  $\text{erg} \cdot \text{s}^{-1} \cdot \text{cm}^{-2}$ .

The latter is given by  $f_X = ECF \cdot Z$ , where  $ECF$  is the energy conversion factor and  $Z$  is the background and vignetting corrected broad band X-ray count rate.

The  $ECF$  was derived for each source using the “X-ray colours”, or hardness ratios,  $HR1$  and  $HR2$  in the same way as described in Neuhäuser et al. (1995b) and Alcalá et al. (1997)<sup>2</sup>. The relevant X-ray data are presented in Table 3. Except for three X-ray sources, discussed in Sect. 5, most of the sources have hardness ratios that are consistent with those of PMS stars (see Fig. 4 in Sect. 5).

The X-ray luminosities  $L_X$ , listed in Column (8) of Table 3, are computed adopting a distance of 200 pc for the Cha II cloud (Hughes and Hartigan 1992) and assuming that all the X-ray sources are located at the distance of Cha II, which might not be the case for background or foreground sources. However, once the distance to those objects should be known, their X-ray luminosities can be easily scaled from those listed in Table 3.

Of the 47 PMS stars and IRAS sources that fall in the area of the ROSAT observation, 34 were not detected. For these objects, we have derived upper limits to the X-ray count rates and, using a mean  $ECF$  of  $1.2 \times 10^{-11} \text{ erg} \cdot \text{sec} \cdot \text{cm}^{-2} \cdot \text{count}^{-1}$  computed from the  $ECF$  values reported in Table 3, we derive upper limits for their X-ray luminosity.

In Table 4 a compilation of the 49 YSOs in the Cha II cloud is reported. The X-ray luminosities for the stars detected and the upper limits for those objects not detected are listed in Column (4)<sup>3</sup>. The CTTS Sz64 and the IR source IRAS 13047-7750 lie outside the area of the X-ray pointing and that is why no upper limit for their X-ray luminosity is reported.

The stars with the highest X-ray luminosities are RXJ 1301.0-7654a, RXJ 1303.1-7706, CM Cha and Hn22 & Hn23. We remind the reader that RXJ 1301.0-7654a is a PMS spectroscopic binary (Covino et al. 1997) and a visual double (Brandner et al. 1996). Thus, this star is probably a hierarchical triple system in which the combination of the individual X-ray luminosities of the three components results in a high level of X-ray emission. On the other hand, since the resolution of the PSPC is not sufficient to resolve Hn22 from Hn23, their X-ray luminosity should also be considered as an upper limit. For RXJ 1303.1-7706 and CM Cha there is no information on binarity neither do we find evidence of variability in their X-ray light curves. Hence, the latter two stars are intrinsically X-ray bright.

## 5. Discussion

Except for two objects, practically all YSOs in Cha II lie in the area of the ROSAT pointing. This provides us with a spatially complete sample and a good census of the X-ray emitting population of Cha II.

Class-III IR sources or WTTS show-up preferentially in X-rays. From previous ROSAT studies in SFRs, it was found that

<sup>2</sup> for the definition of the hardness ratios  $HR1$  and  $HR2$  see Zimmernann et al. (1993)

<sup>3</sup> Ambiguous identifications (see Sect. 3), e.g. Hn22 and Hn23, are considered as upper limits too.

**Table 3.** X-ray properties of the sources detected in the ROSAT pointed observation in the Chamaeleon II dark cloud. The columns are: (1) CHIIRX running number from Table 1; (2) Hardness ratio 1; (3) Hardness ratio 2; (4) X-ray emission energy in  $keV$ ; (5) Logarithm of Hydrogen column density in  $cm^{-2}$ ; (6) Energy conversion factor in  $10^{-11} \text{ erg sec}^{-1} \text{ cm}^{-2} \text{ count}^{-1}$ ; (7) X-ray flux in  $10^{-14} \text{ erg sec}^{-1} \text{ cm}^{-2}$ ; (8) Logarithm of X-ray luminosity in  $\text{erg sec}^{-1}$  and (9) identification from Table 1.

CHIIRX (1)	HR1 (2)	HR2 (3)	$k \cdot T_X$ (4)	$\log N_H$ (5)	ECF (6)	$f_X$ (7)	$\log L_X$ (8)	IDENT (9)
1	1.00±0.00	0.27±0.21	0.50 <sup>+1.52</sup> <sub>-0.33</sub>	21.95 <sup>+0.05</sup> <sub>-3.95</sub>	1.09 <sup>+0.35</sup> <sub>-0.26</sub>	3.83 <sup>+2.29</sup> <sub>-1.51</sub>	29.26 <sup>+0.22</sup> <sub>-0.21</sub>	Sz46N
2	1.00±0.00	0.61±0.24	1.62 <sup>+0.40</sup> <sub>-1.05</sub>	21.50 <sup>+0.50</sup> <sub>-3.50</sub>	1.46 <sup>+1.05</sup> <sub>-0.54</sub>	4.18 <sup>+5.10</sup> <sub>-2.32</sub>	29.30 <sup>+0.35</sup> <sub>-0.35</sub>	IRAS 12535-7623
3	1.00±0.00	1.00±0.00	0.04 <sup>+1.98</sup> <sub>-0.00</sub>	18.00 <sup>+4.00</sup> <sub>-0.00</sub>	1.24 <sup>+3.06</sup> <sub>-0.98</sub>	1.85 <sup>+6.22</sup> <sub>-1.56</sub>	28.95 <sup>+0.81</sup> <sub>-0.64</sub>	IRAS 12551-7657?
4	1.00±0.00	0.81±0.29	1.74 <sup>+0.28</sup> <sub>-0.88</sub>	21.95 <sup>+0.05</sup> <sub>-0.75</sub>	2.18 <sup>+0.33</sup> <sub>-0.95</sub>	6.95 <sup>+3.34</sup> <sub>-4.16</sub>	29.52 <sup>+0.39</sup> <sub>-0.17</sub>	
5	1.00±0.00	0.14±0.37	1.00 <sup>+1.02</sup> <sub>-0.90</sub>	19.75 <sup>+2.25</sup> <sub>-1.75</sub>	0.86 <sup>+0.60</sup> <sub>-0.07</sub>	0.70 <sup>+0.92</sup> <sub>-0.29</sub>	28.52 <sup>+0.23</sup> <sub>-0.37</sub>	
6	1.00±0.00	0.19±0.43	1.03 <sup>+0.99</sup> <sub>-0.93</sub>	20.65 <sup>+1.35</sup> <sub>-2.65</sub>	0.97 <sup>+0.64</sup> <sub>-0.19</sub>	7.05 <sup>+7.21</sup> <sub>-2.62</sub>	29.53 <sup>+0.20</sup> <sub>-0.31</sub>	
7	1.00±0.00	0.56±0.10	1.08 <sup>+0.94</sup> <sub>-0.33</sub>	21.85 <sup>+0.15</sup> <sub>-0.19</sub>	1.34 <sup>+0.31</sup> <sub>-0.19</sub>	1.66 <sup>+0.93</sup> <sub>-0.62</sub>	28.90 <sup>+0.20</sup> <sub>-0.19</sub>	Sz48NE
8	0.99±0.07	0.25±0.11	0.60 <sup>+0.59</sup> <sub>-0.36</sub>	21.90 <sup>+0.10</sup> <sub>-1.20</sub>	1.09 <sup>+0.10</sup> <sub>-0.16</sub>	6.93 <sup>+1.54</sup> <sub>-1.72</sub>	29.52 <sup>+0.12</sup> <sub>-0.09</sub>	Sz50
9	0.96±0.01	0.17±0.03	0.98 <sup>+0.03</sup> <sub>-0.06</sub>	20.95 <sup>+0.35</sup> <sub>-0.05</sub>	0.96 <sup>+0.01</sup> <sub>-0.01</sub>	92.24 <sup>+4.23</sup> <sub>-4.04</sub>	30.64 <sup>+0.02</sup> <sub>-0.02</sub>	RXJ 1301.0-7654a
10	0.97±0.13	0.85±0.09	2.02 <sup>+0.00</sup> <sub>-0.70</sub>	22.00 <sup>+0.00</sup> <sub>-0.15</sub>	2.51 <sup>+0.00</sup> <sub>-0.60</sub>	10.17 <sup>+1.51</sup> <sub>-3.60</sub>	29.69 <sup>+0.19</sup> <sub>-0.06</sub>	IRAS F12571-7657
11	0.35±0.55	1.00±0.00	1.08 <sup>+0.94</sup> <sub>-1.04</sub>	18.40 <sup>+3.60</sup> <sub>-0.40</sub>	0.89 <sup>+3.41</sup> <sub>-0.19</sub>	0.41 <sup>+2.46</sup> <sub>-0.23</sub>	28.29 <sup>+0.35</sup> <sub>-0.84</sub>	
12	0.55±0.30	0.35±0.24	1.33 <sup>+0.69</sup> <sub>-0.36</sub>	20.00 <sup>+0.65</sup> <sub>-2.00</sub>	0.99 <sup>+0.38</sup> <sub>-0.15</sub>	1.71 <sup>+1.26</sup> <sub>-0.63</sub>	28.91 <sup>+0.20</sup> <sub>-0.24</sub>	IRAS 12583-7634
13	1.00±0.00	0.35±0.07	1.25 <sup>+0.77</sup> <sub>-0.89</sub>	20.60 <sup>+1.40</sup> <sub>-2.60</sub>	1.09 <sup>+0.29</sup> <sub>-0.21</sub>	26.53 <sup>+9.41</sup> <sub>-6.69</sub>	30.10 <sup>+0.12</sup> <sub>-0.13</sub>	CM Cha
14	0.72±0.65	0.66±0.34	1.79 <sup>+0.23</sup> <sub>-1.26</sub>	21.60 <sup>+0.40</sup> <sub>-1.80</sub>	1.61 <sup>+0.89</sup> <sub>-0.66</sub>	1.34 <sup>+1.54</sup> <sub>-0.85</sub>	28.81 <sup>+0.44</sup> <sub>-0.33</sub>	
15	1.00±0.00	1.00±0.00	0.04 <sup>+1.98</sup> <sub>-0.00</sub>	18.00 <sup>+4.00</sup> <sub>-0.00</sub>	1.24 <sup>+3.06</sup> <sub>-0.98</sub>	0.63 <sup>+2.51</sup> <sub>-0.55</sub>	28.48 <sup>+0.93</sup> <sub>-0.70</sub>	
16	1.00±0.00	-0.49±0.38	0.27 <sup>+0.47</sup> <sub>-0.22</sub>	20.20 <sup>+1.80</sup> <sub>-2.20</sub>	0.92 <sup>+1.15</sup> <sub>-0.54</sub>	0.49 <sup>+1.09</sup> <sub>-0.38</sub>	28.37 <sup>+0.64</sup> <sub>-0.51</sub>	
17	0.34±0.31	-0.16±0.29	0.50 <sup>+0.47</sup> <sub>-0.20</sub>	18.00 <sup>+2.20</sup> <sub>-0.00</sub>	0.77 <sup>+3.41</sup> <sub>-0.04</sub>	1.02 <sup>+0.52</sup> <sub>-0.33</sub>	28.68 <sup>+0.17</sup> <sub>-0.18</sub>	
18	0.97±0.02	0.22±0.05	1.00 <sup>+0.07</sup> <sub>-0.74</sub>	21.15 <sup>+0.85</sup> <sub>-0.25</sub>	0.98 <sup>+0.12</sup> <sub>-0.04</sub>	34.98 <sup>+6.09</sup> <sub>-3.01</sub>	30.22 <sup>+0.04</sup> <sub>-0.07</sub>	RXJ 1303.1-7706
19	0.97±0.44	0.36±0.29	1.18 <sup>+0.84</sup> <sub>-0.99</sub>	21.10 <sup>+0.90</sup> <sub>-1.25</sub>	1.08 <sup>+0.57</sup> <sub>-0.20</sub>	1.28 <sup>+1.26</sup> <sub>-0.55</sub>	28.79 <sup>+0.24</sup> <sub>-0.30</sub>	
20	0.98±0.03	0.44±0.07	1.21 <sup>+0.81</sup> <sub>-0.63</sub>	21.35 <sup>+0.65</sup> <sub>-0.45</sub>	1.14 <sup>+0.31</sup> <sub>-0.06</sub>	18.28 <sup>+6.67</sup> <sub>-2.30</sub>	29.94 <sup>+0.06</sup> <sub>-0.14</sub>	
21	1.00±0.00	0.86±0.32	2.02 <sup>+0.00</sup> <sub>-1.12</sub>	22.00 <sup>+0.00</sup> <sub>-0.70</sub>	2.51 <sup>+0.00</sup> <sub>-1.24</sub>	1.79 <sup>+0.74</sup> <sub>-1.26</sub>	28.93 <sup>+0.52</sup> <sub>-0.15</sub>	
22	1.00±0.00	0.06±0.27	0.92 <sup>+0.36</sup> <sub>-0.82</sub>	19.85 <sup>+2.15</sup> <sub>-1.85</sub>	0.85 <sup>+0.30</sup> <sub>-0.06</sub>	1.75 <sup>+1.26</sup> <sub>-0.56</sub>	28.92 <sup>+0.17</sup> <sub>-0.24</sub>	
23	1.00±0.00	1.00±0.00	0.04 <sup>+1.98</sup> <sub>-0.00</sub>	18.00 <sup>+4.00</sup> <sub>-0.00</sub>	1.24 <sup>+3.06</sup> <sub>-0.98</sub>	1.49 <sup>+5.65</sup> <sub>-1.30</sub>	28.85 <sup>+0.89</sup> <sub>-0.68</sub>	
24	0.86±0.13	0.24±0.13	1.10 <sup>+0.22</sup> <sub>-0.84</sub>	20.50 <sup>+1.90</sup> <sub>-0.30</sub>	0.99 <sup>+0.14</sup> <sub>-0.08</sub>	4.87 <sup>+1.42</sup> <sub>-1.00</sub>	29.37 <sup>+0.10</sup> <sub>-0.11</sub>	
25	1.00±0.00	0.44±0.35	1.24 <sup>+0.78</sup> <sub>-1.04</sub>	21.30 <sup>+0.70</sup> <sub>-3.30</sub>	1.15 <sup>+1.00</sup> <sub>-0.31</sub>	0.96 <sup>+1.51</sup> <sub>-0.52</sub>	28.66 <sup>+0.34</sup> <sub>-0.41</sub>	
26	-0.35±0.26	-0.01±0.44	0.25 <sup>+1.77</sup> <sub>-0.15</sub>	18.00 <sup>+2.90</sup> <sub>-0.00</sub>	0.69 <sup>+0.80</sup> <sub>-0.11</sub>	1.42 <sup>+2.53</sup> <sub>-0.57</sub>	28.83 <sup>+0.22</sup> <sub>-0.44</sub>	
27	0.96±0.02	0.28±0.05	1.10 <sup>+0.06</sup> <sub>-0.78</sub>	20.95 <sup>+1.05</sup> <sub>-0.15</sub>	1.03 <sup>+0.12</sup> <sub>-0.04</sub>	51.03 <sup>+8.55</sup> <sub>-4.23</sub>	30.39 <sup>+0.04</sup> <sub>-0.07</sub>	Hn22 & Hn23
28	0.88±0.20	0.56±0.15	2.02 <sup>+0.00</sup> <sub>-1.31</sub>	21.35 <sup>+0.65</sup> <sub>-0.70</sub>	1.53 <sup>+0.23</sup> <sub>-0.39</sub>	5.00 <sup>+1.78</sup> <sub>-1.95</sub>	29.38 <sup>+0.21</sup> <sub>-0.13</sub>	
29	1.00±0.00	1.00±0.00	0.04 <sup>+1.98</sup> <sub>-0.00</sub>	18.00 <sup>+4.00</sup> <sub>-0.00</sub>	1.24 <sup>+3.06</sup> <sub>-0.98</sub>	0.81 <sup>+3.19</sup> <sub>-0.71</sub>	28.59 <sup>+0.91</sup> <sub>-0.69</sub>	Sz54
30	1.00±0.00	0.52±0.07	1.67 <sup>+0.35</sup> <sub>-0.93</sub>	21.20 <sup>+0.80</sup> <sub>-0.30</sub>	1.37 <sup>+0.16</sup> <sub>-0.22</sub>	40.18 <sup>+8.10</sup> <sub>-9.05</sub>	30.28 <sup>+0.11</sup> <sub>-0.08</sub>	
31	1.00±0.00	0.52±0.26	1.86 <sup>+0.16</sup> <sub>-1.53</sub>	21.20 <sup>+0.80</sup> <sub>-3.20</sub>	1.43 <sup>+0.65</sup> <sub>-0.56</sub>	6.17 <sup>+5.05</sup> <sub>-3.35</sub>	29.47 <sup>+0.34</sup> <sub>-0.26</sub>	
32	1.00±0.00	0.09±0.15	0.64 <sup>+0.49</sup> <sub>-0.52</sub>	21.70 <sup>+0.30</sup> <sub>-3.70</sub>	0.98 <sup>+0.10</sup> <sub>-0.16</sub>	5.46 <sup>+1.50</sup> <sub>-1.57</sub>	29.42 <sup>+0.15</sup> <sub>-0.11</sub>	
33	-0.08±0.04	0.09±0.06	2.02 <sup>+0.02</sup> <sub>-0.00</sub>	18.00 <sup>+0.00</sup> <sub>-0.00</sub>	0.94 <sup>+0.94</sup> <sub>-0.94</sub>	144.7 <sup>+0.00</sup> <sub>-0.00</sub>	30.84 <sup>+0.00</sup> <sub>-0.00</sub>	HD113513
34	0.81±0.36	0.76±0.25	2.02 <sup>+0.00</sup> <sub>-1.11</sub>	21.80 <sup>+0.20</sup> <sub>-0.50</sub>	1.98 <sup>+0.52</sup> <sub>-0.71</sub>	4.60 <sup>+2.69</sup> <sub>-2.41</sub>	29.34 <sup>+0.32</sup> <sub>-0.20</sub>	Sz57
35	1.00±0.00	0.79±0.39	1.56 <sup>+0.46</sup> <sub>-0.90</sub>	21.95 <sup>+0.05</sup> <sub>-1.40</sub>	2.05 <sup>+0.46</sup> <sub>-0.94</sub>	1.68 <sup>+1.21</sup> <sub>-1.14</sub>	28.90 <sup>+0.49</sup> <sub>-0.24</sub>	
36	-0.35±0.21	-0.27±0.41	0.24 <sup>+0.03</sup> <sub>-0.04</sub>	18.00 <sup>+2.10</sup> <sub>-0.00</sub>	0.69 <sup>+0.15</sup> <sub>-0.03</sub>	3.67 <sup>+1.68</sup> <sub>-0.92</sub>	29.24 <sup>+0.12</sup> <sub>-0.17</sub>	
37	1.00±0.00	0.12±0.22	0.78 <sup>+0.52</sup> <sub>-0.67</sub>	21.55 <sup>+0.45</sup> <sub>-3.55</sub>	0.96 <sup>+0.20</sup> <sub>-0.14</sub>	3.58 <sup>+1.71</sup> <sub>-1.21</sub>	29.23 <sup>+0.18</sup> <sub>-0.17</sub>	IRAS F1352-7653
38	1.00±0.00	0.63±0.41	1.61 <sup>+0.41</sup> <sub>-1.32</sub>	21.55 <sup>+0.45</sup> <sub>-3.55</sub>	1.49 <sup>+1.02</sup> <sub>-0.62</sub>	3.43 <sup>+4.28</sup> <sub>-2.10</sub>	29.21 <sup>+0.41</sup> <sub>-0.35</sub>	
39	1.00±0.00	0.15±0.17	1.01 <sup>+0.24</sup> <sub>-0.89</sub>	19.20 <sup>+2.80</sup> <sub>-1.20</sub>	0.85 <sup>+0.29</sup> <sub>-0.03</sub>	5.57 <sup>+3.24</sup> <sub>-1.15</sub>	29.42 <sup>+0.10</sup> <sub>-0.20</sub>	
40	1.00±0.00	0.18±0.20	1.04 <sup>+0.98</sup> <sub>-0.92</sub>	20.05 <sup>+1.95</sup> <sub>-2.05</sub>	0.90 <sup>+0.35</sup> <sub>-0.08</sub>	6.41 <sup>+4.47</sup> <sub>-1.89</sub>	29.49 <sup>+0.15</sup> <sub>-0.23</sub>	

YSOs have hardness ratios typically in the ranges  $-0.15 < HR1 < 1$  and  $-0.3 < HR2 < 0.5$  (Neuhäuser et al. 1995a). This, of course, does not exclude that other active field stars may contaminate samples of X-ray selected sources with hardness ratios that fall in the box defined above. However, it is a starting point to pre-select objects with X-ray characteristics similar to those of active stars and in particular to those of YSOs.

In Fig. 4 the hardness ratio diagram, HR2 versus HR1 is shown. The objects identified with previously known YSOs are indicated with shaded circles, while the remaining X-ray sources

are marked with crosses. Many of the X-ray sources identified with YSOs in the Cha II pointing have hardness ratios that fall in the box defined above. Note, however, that some of them have  $HR2 > 0.5$ , but this also happens in the sample of YSOs by Neuhäuser et al. (1995a; see their Fig. 1). Thus some YSOs may still have  $HR2 > 0.5$  (but  $HR1 > 0.5$ ). Also three of the newly identified lithium stars (indicated with a dot in Fig. 4) satisfy the hardness ratio criterion.

Three X-ray sources with  $HR1 < 0$  have hardness ratios inconsistent with those of YSOs. Two of them, CHIIR-33

**Table 4.** Young stellar objects in the Chamaeleon II dark cloud and their X-ray luminosities.

Star	CHII-	IR	$\log L_X$ [erg/sec]	other designation	ref.
	XR	Class			
Sz 46N1	1	II	29.26		1
Sz 47		II	<29.25		1
Sz 48NE	7	II	28.90		1
Sz 49		II	<29.50		1
Sz 50	8	II	29.52	12571-7654	1
RXJ1301.0-7654a	9	III	30.64		4
Sz51		II	<29.55	BC Cha	1
RXJ1303.1-7706	18	III	30.22		4
CM Cha	13	II	30.10	12584-7621	1
Sz 52		II	<30.86		1
Hn 22	27	II	<30.39	13005-7633	2
Hn 23	27	II	<30.39	13005-7633	2
Hn 24		III	<30.57		2
Hn 25		II	<29.20		2
Sz 53		II	<29.02		1
Sz 54	29	II	28.59	BF Cha	1
Sz 55		II	<28.89		1
Sz 56		II	<29.41		1
Sz 57	34	II	29.34	13030-7707	1
Sz 58		II	<29.63	13030-7707	1
Sz 59		II	<29.43	BK Cha	1
Sz 60W		II	<29.27		1
Sz 60E		II	<29.27		1
Hn 26		III	<29.13		2
Sz 61		II	<31.03	BM Cha	1
Sz 62		II	<32.40		1
Sz 63		II	<29.75		1
Sz 64 <sup>†</sup>		II	–		1
IRAS 12496-7650		I	<29.00		6
IRAS 12500-7658		I	<29.34		5
* IRAS 12506-7730			<29.72		3
* IRAS 12510-7631			<29.50		3
* IRAS 12510-7718			<29.32		3
IRAS 12522-7640			<29.04		3
IRAS 12533-7632		I	<28.80		5
IRAS 12535-7623	2	II	29.30		5
* IRAS 12539-7627			<28.95		3
* IRAS 12551-7657	3?		28.95		3
IRAS 12553-7651		I	<28.65		5
IRAS 12554-7635		II	<28.52		5
IRAS F12555-7638		II	<29.50		5
IRAS 12556-7731		II	<29.50		5
IRAS F12571-7657	10	II	29.69		5
* IRAS 12583-7634	12		28.91		3
* IRAS 12591-7719			<28.76		3
* IRAS 12594-7707			<28.38		3
IRAS 13036-7644		I	<28.83		3
* IRAS 13047-7750 <sup>†</sup>			–		3
IRAS F13052-7653	37	II	29.23		5

references: 1) Hughes & Hartigan 1992; 2) Hartigan 1993; 3) Schwartz 1991; 4) Alcalá et al. 1995; 5) Prusti et al. 1992; 6) Whittet et al. 1991

\*: Weak IR source, detected only in  $100\mu$  (Schwartz 1991); †: object outside ROSAT pointed area.

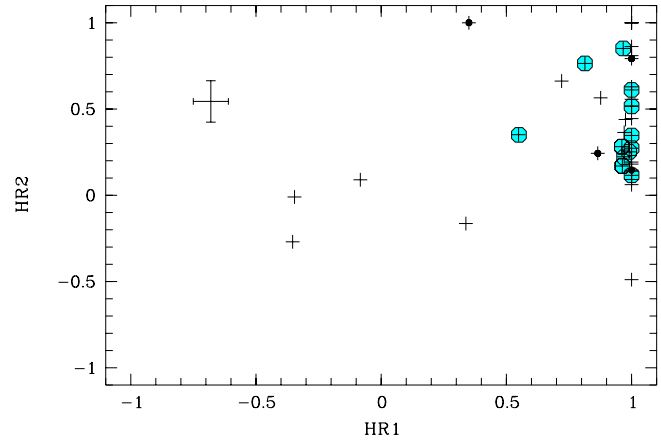


**Fig. 4.** Scatter plot of HR2 versus HR1 for the ROSAT pointing sources listed in Tables 1 and 2. The shaded circles represent the sources identified with previously known YSOs in Cha II. The newly identified lithium stars (see Sect. 3) are marked with a black dot. The mean errors of HR1 and HR2 are also indicated.

and CHII-XR-36, are identified with the stars HD113513 and HD113696 respectively, which are not related to the Cha II cloud. In the error box of the other source (CHII-XR-26) there are faint objects in the centre of the field which may be foreground or background objects.

From the similarities between the X-ray properties of the sources not yet optically identified (represented with crosses in Fig. 4) and those of the YSOs in Cha II and in other SFRs, it is expected that several of them will have a YSO counterpart. In any case, because of the small number of sources left, the result that in Cha II the CTTS may be more numerous than the WTTS prevails.

An alternative hypothesis is that WTTS in Cha II may be more numerous than those detected in this study, but they are embedded or lie behind the dark cloud with their X-ray emission being screened by several magnitudes of extinction. Note that most of the known YSOs in Cha II lie on the western side of the dark cloud, which leads to the idea that we are mainly detecting the less “obscured edge” of the entire population of YSOs. However, since in hard X-rays the absorption is lower than in the optical (for the hard band  $A_V = 5$  means  $A_X \approx 1$ ), 1-2 keV photons can reach us even from embedded objects with up to 10 - 15 mags. of visual extinction, which makes possible the X-ray detection of embedded IR sources in hard X-rays (Casanova et al. 1995; Montmerle 1996). Therefore, if there were many embedded or screened X-ray emitting YSOs in Cha II, at least some of them would have been detected in the deep ASCA observation by Yamauchi et al. (1998). In fact, the Herbig Ae star IRAS 12496-7650 was detected by ASCA despite more than 100 magnitudes of extinction<sup>4</sup>.

<sup>4</sup> We derived  $A_V$  using the Hydrogen column density value of  $N_H \approx 2 \times 10^{23} \text{cm}^{-2}$  reported by Yamauchi et al. (1998) and the relation  $N_H = 1.79 \cdot A_V \times 10^{21} \text{cm}^{-2}$  by Predehl and Schmitt (1995). The Yamauchi et al. (1998) X-ray spectrum for this star (their source

Another possibility is that the X-ray fluxes of many WTTS fall below the detection limit of the ASCA and ROSAT observations. There may be two possible explanations for this: first, there is clear evidence that the Cha II cloud is located farther away than 180 pc. X-ray emitting YSOs with X-ray fluxes below  $10^{-14} \text{ erg} \cdot \text{sec}^{-1} \cdot \text{cm}^{-2}$ , which is the limiting flux of our ROSAT pointing at a distance of 200 pc of the Cha II cloud (Hughes and Hartigan 1992), would escape from detection; second, the mass function of the Cha II cloud indicates that there is a larger fraction of low-mass stars in Cha II than in the Cha I SFR (Hughes and Hartigan 1992). Therefore, the strong dependence of the X-ray luminosity on the mass (Feigelson et al. 1993; Walter 1996), would make difficult the X-ray detection of PMS stars with masses lower than about  $0.15 M_{\odot}$ . In fact, the X-ray luminosities of the Cha II objects are apparently consistent with low masses<sup>5</sup>. In order for these two effects to explain the paucity of WTTS and the low WTTS/CTTS ratio, the WTTS would have to be intrinsically less X-ray bright than CTTS. However, this is not generally the case. Therefore, we conclude that the low WTTS/CTTS ratio in Cha II is real.

We have attempted to determine an X-ray luminosity function (XLF), using the data listed in Table 4, but the fact that 70% of the X-ray luminosities are upper-limits leads to a bias in the XLF.

The comparison with the XLF of the Cha I sample, derived using the X-ray luminosities reported by Feigelson et al. (1993) and including the lithium stars identified by Lawson, Feigelson and Huenemoerder (1996), shows that there is a slight trend for the Cha I sample to have a higher level of X-ray emission (c.f. Fig. 5). The mean X-ray luminosity of the Cha II members ( $\langle \log L_X \rangle = 28.86 \pm 0.10$ ) is slightly lower than that for the Cha I members ( $\langle \log L_X \rangle = 29.20 \pm 0.05$ ). This difference may again reflect the strong dependence of X-ray luminosity on mass (Feigelson et al. 1993; Walter et al. 1996) as a consequence of the fact that there is a larger fraction of low-mass stars in Cha II than there is in Cha I.

On the other hand, the comparison of the age distributions of the Cha I and Cha II stars, shows that the Cha II stars are, on average, younger than those of Cha I (see Fig. 7 by Alcalá et al. 1997) and, hence, it is likely that Cha II is in an earlier evolutionary stage than Cha I (Gauvin and Strom 1992 and Prusti et al. 1992). Assuming the scenario in which CTTS eventually evolve into WTTS by the dispersion of their circumstellar disk or the formation of planets, then in Cha II one would expect the ratio  $\text{No.}(WTTS)/\text{No.}(CTTS)$  to be less than in Cha I, as a consequence of the different evolutionary status of the two regions. Such scenario would be consistent with the low detection rate of WTTS in the ROSAT pointed observation.

No. 1), in which almost no emission is seen from 0.5 to 2 keV, explains the non-detection by ROSAT.

<sup>5</sup> Note that a larger distance of the Cha II cloud would move the early type stars to higher masses on the HR diagram. However, the stars in Cha II are typically of late spectral type, and the corresponding PMS evolutionary tracks run almost vertically on the HR diagram. Hence, the uncertainty on the distance does not affect the derived mass significantly.

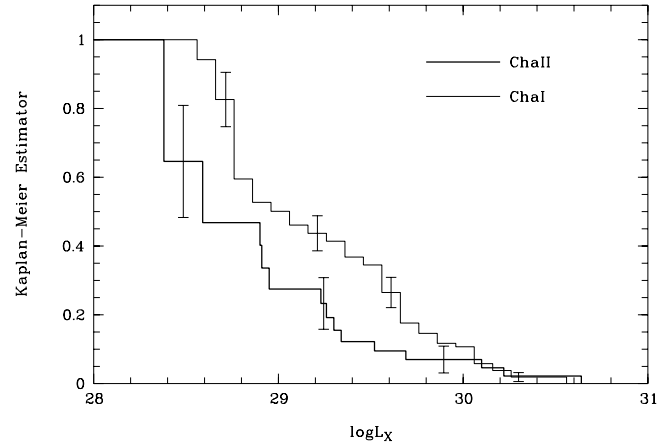


**Fig. 5.** Kaplan-Meier X-ray luminosity functions of PMS stars in the Cha II cloud (thick line) and Cha I cloud (thin line).

The non detection of any of the protostar candidates in Cha II in the ROSAT pointing, which is in line with the ASCA results by Yamauchi et al. (1998), might in principle be attributed to their X-ray variability but, it is hard to believe that X-ray variability is the reason for the non detection of all five protostar candidates in two X-ray observations. We think that the probability to detect X-ray emission from a protostar, where the “circum-protostellar” matter should be distributed more in a torus-like structure than in a disk, is intrinsically low because a small angle of the polar axis with respect to the line of sight would be sufficient for the protostellar matter to screen the X-ray emission. In this sense, the non detection of any of the protostar candidates might be consistent with the possibility that the class-I IR sources in Cha II are seen most likely edge-on, as proposed by Yamauchi et al. (1998).

## 6. Conclusions

Our ROSAT pointed observation in the Cha II dark cloud revealed 40 X-ray sources with high confidence, of which 35% were identified with YSOs. Of the 49 Cha II optical and IR members, 14 were detected in X-rays. None of the protostellar candidates in Cha II was detected in X-rays. On the basis of intermediate resolution spectroscopy, four new WTTS candidates were found. Most of the X-ray sources detected lie in the eastern side of the Cha II cloud. The north-west part of the cloud is devoid both in X-ray sources and visible PMS stars. The stars in Cha II are typically less X-ray luminous than those in Cha I. This result, together with the strong dependence of the X-ray luminosity on stellar mass, is consistent with the fact that the mass spectrum in the Cha II cloud is biased towards less massive stars. An important result of our X-ray observation in Cha II is that the number of class-III IR sources or WTTS is less than that of class-II IR sources or CTTS, contrary to the results of previous investigations in the Cha I cloud, where WTTS outnumber CTTS at least by a factor of 2. This probably indicates an earlier evolutionary stage for Cha II relative to Cha I.

*Acknowledgements.* We thank the referee, Dr. K. Smith, for valuable comments and suggestions. The ROSAT project has been supported by the Bundesministerium für Bildung, Wissenschaft, Forschung und Technologie and the Max-Planck-Gesellschaft.

## References

- Alcalá J.M., Krautter J., Schmitt J.H.M.M., et al., 1995, *A&AS* 114, 109
- Alcalá J.M., Krautter J., Covino E., et al., 1997, *A&A* 319, 184
- Alcalá J.M., Covino E., Torres G., et al., 2000, *A&A* 353, 186
- Brandner W., Alcalá J.M., Munkel M., Moneti A., Zinnecker H., 1996, *A&A* 307, 121
- Briceño C., Hartmann L.W., Stauffer J.R., et al., 1997, *AJ* 113, 740
- Casanova S., Montmerle T., Feigelson E.D., André P., 1995, *ApJ* 439, 752
- Covino E., Alcalá J.M., Allain S., et al., 1997, *A&A* 328, 187
- Favata F., Micela G., Sciortino S., 1997, *A&A* 326, 647
- Feigelson E.D., Kriss G.A., 1989, *ApJ* 338, 262
- Feigelson E.D., Casanova S., Montmerle T., Guibert J., 1993, *ApJ* 416, 623
- Gauvin L.S., Strom K., 1992, *ApJ* 385, 217
- Grosso N., Montmerle T., Feigelson E.D., et al., 1997, *Nat* 387, 56
- Hartigan P., 1993, *AJ* 105, 1511
- Hoffmeister C., 1963, *Veröf. Stern. Sonneberg* 6, 63
- Hughes J., Hartigan P., 1992, *AJ* 104, 680
- Kamata Y., Koyama K., Tsuboi Y., Yamauchi S., 1997, *PASJ* 49, 461
- Koyama K., Maeda Y., Ozaki M., et al., 1994, *PASJ* 46, L25
- Koyama K., Hamaguchi K., Ueno S., Kobayashi N., Feigelson E.D., 1996, *PASJ* 48, L87
- Krautter J., Alcalá J.M., Wichmann R., Neuhäuser R., Schmitt J.H.M.M., 1994, *Rev. Mex. Astron. Astrofis.* 29, 41
- Larson K.A., Whittet D.C.B., Prusti T., Chiar J.E., 1998, *A&A* 337, 465
- Lawson A.W., Feigelson E.D., Huenemoerder D.P., 1996, *MNRAS* 280, 1071
- Montmerle T., Koch-Miramond L., Falgarone E., Grindlay J.E., 1983, *ApJ* 269, 182
- Montmerle T., 1996, In: Pallavicini R., Dupree A.K. (eds.) *Cool Stars, Stellar Systems, and The Sun. Ninth Cambridge Workshop*, p. 405
- Neuhäuser R., Sterzik M.F., Schmitt J.H.M.M., Wichmann R., Krautter J., 1995a, *A&A* 295, L5
- Neuhäuser R., Sterzik M.F., Schmitt J.H.M.M., Wichmann R., Krautter J., 1995b, *A&A* 297, 391
- Neuhäuser R., Preibisch Th., 1997, *A&A* 322, L37
- Predehl P., Schmitt J.H.M.M., 1995, *A&A* 293, 889
- Prusti T., Whittet D.C.B., Assendorp R., Wesselius P.R., 1992, *A&A* 260, 151
- Schwartz R.D., 1977, *ApJS* 35, 161
- Schwartz R.D., 1991, In: Reipurth B. (ed.) *Low Mass Star Formation in Southern Molecular Clouds*. ESO rept. No. 11, ESO, Garching, p. 93
- Walter F.M., Brown A., Mathieu R.D., Myers P.C., Vrba F.J., 1988, *AJ* 96, 297
- Walter F.M., 1996, In: Pallavicini R., Dupree A.K. (eds.) *Cool Stars, Stellar Systems, and The Sun. Ninth Cambridge Workshop*, p. 441
- Walter F.M., Alcalá J.M., Neuhäuser R., Sterzik M.F., Wolk S.J., 1999, *The low-mass stellar population of the Orion OB1 association and implications for the formation of low-mass stars*. In: *Protostars & Planets IV*, Univ. of Arizona Press, Tucson, in press
- Whittet D.C.B., Assendorp R., Prusti T., Roth M., Wesselius P.R., 1991, *A&A* 251, 524
- Wichmann R., Covino E., Alcalá J.M., et al., 1999, *MNRAS*, in press
- Yamauchi S., Hamaguchi K., Koyama K., Murakami H., 1998, *PASJ* 50, 465
- Zimmermann H.U., et al., 1993, *EXSAS User's Guide MPE report No.* 244